Elucidation of the mechanism of single-stranded DNA interaction with methylene blue. A spectroscopic approach.

Mayreli Ortiz,[a,*] Alex Fragoso,[a] Pedro J. Ortiz[b] and Ciara K. O´Sullivan[a,c*]

[a] Nanobiotechnology & Bioanalysis Group, Departament d'Enginyeria Química, Universitat Rovira i Virgili, Avinguda Països Catalans 26, 43007 Tarragona, Spain

[b] Department of Physical-Chemistry, Faculty of Chemistry, Universidad de La Habana, Havana 10400, Cuba.

[c] Institució Catalana de Recerca i Estudis Avançats, Passeig Lluís Companys, 23, 08010 Barcelona, Spain.

Corresponding author: Mayreli Ortiz, Ciara K. O'Sullivan, Departament d'Enginyeria Química, Universitat Rovira i Virgili, Avinguda Països Catalans 26, 43007 Tarragona, Spain. Tel: +34 977558740 Fax: +34 977559667. e-mail: mayreli.ortiz@urv.cat, ciara.osullivan@urv.cat

Abstract

The interaction of photosensitizer methylene blue (MB) with single stranded oligonucleotides of composition AAA-AAA-AAA (A_9), CCC-CCC-CCC (C_9), GGG-GGG-GGG (G_9), and TTT-TTT-TTT (T_9) has been studied using UV-VIS and fluorescence spectroscopies. The quenching effect of single stranded G_9 over MB is favored over the other sequences. The analysis of the fluorescence data by Benesi-Hildebrand plot shows that MB forms 1:1 complex with G_9. Results from spectroscopic experiments, Stern-Volmer and van't Hoff plots are consistent with a principal contribution of the static quenching on the overall quenching mechanism and with the electrostatic binding mode of MB-single stranded G_9 system. A quantum chemical modelling at DFT//B3LYP/6-31G(d,p) level confirms the experimental results. Asides from providing an insight into the underlying mechanism of the interaction between methylene blue and DNA, these results can be exploited for the design of novel DNA sensors using photoactive labels.

Keywords: methylene blue, DNA, fluorescence, Stern-Volmer plot, electrostatic interactions

Introduction

The study of the interaction of various dye molecules with DNA has been of great interest for a long time due to their importance in the understanding of drug-DNA interactions and the consequent design of new and efficient drugs targeted to DNA [1,2] such as photodynamic therapy (PDT) [3,4] a combined light-plus-drug treatment for malignant tumours.

There are three main models for the binding of a dye to DNA[3,5-9]; intercalative binding, groove (or surface) binding and electrostatic binding. Intercalative binding takes place when a planar, heteroaromatic moiety slides between the DNA base pairs and binds perpendicular to the helix axis. In this type of binding, stacking interactions between the nucleobases and the aromatic ligands play a significant role. Groove binding generally involves direct hydrogen-bonding or van der Waals interactions with the nucleic acid bases in the deep major groove of the DNA helix. In the third type of binding mode, electrostatic interactions between cationic species and the negatively charged DNA phosphate backbone usually occurs along the outside of the helix. From these characteristics, it is apparent that intercalative and groove bindings are related with the grooves in the DNA double helix while the electrostatic binding can take place out of the groove or on the surface of the DNA molecule. However, experimental discrimination of these binding types is difficult [3,10].

Methylene blue (MB) (Scheme 1) is one of the most studied dyes in its interaction with DNA. MB is a photosensitizer that has been extensively used as an optical probe in biophysical systems [11-15] due to its high extinction coefficient that allows it to be used in low concentrations and as such is a good model compound for theoretical studies of the binding types of dyes to DNA [16,17]. In addition, MB is a photosensitizer used to generate singlet oxygen ($^1O_2$) when exposed to both oxygen and

light [18-20]. The interaction of MB with visible light results in oxidative DNA damage, producing predominantly 7,8 dihydro-8-oxoguanine (8-oxo-G) [21-23] and other single base modifications.

Scheme 1.

Different studies have shown that intercalative binding is the dominant mode in MB-dsDNA interaction [7,10,24,25] while minor or major groove and electrostatic bindings can also be observed [16,26]. On the other hand, MB mainly interacts with ssDNA by an electrostatic binding mechanism [26].

MB has also been used as a label for the determination of DNA by electrochemical [24,25, 27] and spectroscopic methods [28,29]. Hu used synchronous fluorescence for the determination of DNA in submicromolar concentrations based on the quenching of MB fluorescence [28]. In another report a nanohybrid consisting of non-luminescent water-soluble CdTe-thioglycolic acid-MB nanocrystals was designed as a label-free signaling platform for DNA based on the reversible restoration of CdTe luminescence in the presence of the target DNA [30]. The system operates better with ds-DNA than with ss-DNA due to the stronger intercalative interaction of MB with ds-DNA, with a detection limit of 42 nM of a 15-mer target sequence. Similar competitive effects on the fluorescence of MB-DNA systems have been used in the study of the interaction of DNA with antibiotics such as daunorubicin [31] and tetracycline [32]. The interaction of DNA with the supramolecular complexes of MB with various neutral and anionic cyclodextrins (CD) has also been recently studied using fluorescence spectroscopy. Stern-Volmer behavior at high [MB]/[DNA] ratios indicated that the quenching of MB

fluorescence by DNA is inhibited by anionic CDs whereas neutral CDs have little influence, supporting an electrostatic mechanism for the MB-DNA interaction [33].

In this work we use UV-VIS and fluorescence spectroscopies to study the interaction of MB with single stranded DNA sequences having the general sequence NNN-NNN-NNN (N9), where N = G (guanine), A (adenine), T (thymine) and C (cytosine). The Stern-Volmer and thermodynamic parameters of the MB-N9 interactions were measured and the effect of salt concentration and pH studied. The results support the existence of a predominantly electrostatic contribution to the overall interaction, where quenching of MB fluorescence is favoured towards the guanine base. The canonical DNA configuration has been used to interpret the results, which is the predominant in Tris-HCl buffer [34] while the ability of guanine-rich sequences to fold into more complex structures called G-quadruplexes [35-39] is also considered to explain the effect of ionic strength in the MB-DNA interaction. Stacking of guanine tetrads into a continuous quadruplex creates cavities within the helix that match the size and geometry for K^+ chelation and, in smaller scale, for Na^+ [40-43].

2 Experimental Section

2.1 Reagents

Methylene blue (MB) was provided by Fluka and purified as described by Bergmann and O'Conski [44]. Fresh stock solutions were prepared before each experiment. The purity of the solution was checked by measuring the A665/A610 ratio, which was always greater than 2.1 indicating the absence of any demethylated methylene blue [44]. The single stranded DNA sequences: AAA-AAA-AAA (A9), CCC-CCC-CCC (C9), GGG-GGG-GGG (G9), and TTT-TTT-TTT (T9) were synthesized by Biomers (Stuttgart, Germany). The samples were reconstituted using Milli-Q water (18.2

MΩ·cm). Tris·HCl was purchased from Sigma Aldrich. All solutions were freshly prepared with Milli-Q water.

2.2 Instrumentation

UV-Vis spectra were recorded at different temperatures in a temperature controlled Cary 100 Bio spectrophotometer (Varian) in 1 cm quartz cells.

The fluorescence experiments were performed at different temperatures in a Cary Eclipse spectrofluorimeter equipped with a Peltier temperature control and regulator. The excitation wavelength was set at 665 nm, which corresponds to the MB-monomer absorption maximum in aqueous solution. The spectra were recorded in the wavelength interval of 670-800 nm with excitation and emission slits of 10 nm and a scan rate of 240 nm/min. All measurements were carried out in triplicate and the average value of the fluorescence changes was used in the calculations. The total volume was corrected for the dilution effect due to the aliquot additions.

2.3 General protocol for spectrophotometric study of interaction of single stranded DNA sequences A_9, C_9, G_9, and T_9 with MB.

A 220 µL aliquot of a freshly prepared 10 µM MB solution in 10 mM Tris·HCl buffer (pH 7.4) + 10 mM NaCl was placed in a quartz cell and titrated with successive 1.2 µL aliquots of 100 µM solution of each DNA sequence, corresponding to 1:0.5; 1:1, 1:1.5 and 1:2 MB:DNA molar ratios. The cell was stirred and the UV-Vis spectrum was recorded after 2 minutes.

2.4 General protocol for fluorescence study of interaction of single stranded DNA sequences: A_9, C_9, G_9, and T_9 with MB.

A 220 μL aliquot of a freshly prepared 5 μM MB solution in 10 mM Tris·HCl buffer (pH 7.4) + 10 mM NaCl was placed in a quartz cell and titrated with a 1.2 μL aliquot of 100 μM solution of each DNA sequence, corresponding to the addition of 1/9 μM DNA (i.e. equivalent to the addition of one nucleotide per MB molecule). The cell was stirred and the UV-Vis spectrum was recorded after 2 minutes. Addition of the 1.2 μL aliquots was repeated 9 times up to a 1:1 MB:DNA molar ratio (corresponding to 9 nucleotides per MB molecule).

2.5 Data treatment

The results were analyzed according both the Stern–Volmer and the modified Stern-Volmer equations. The thermodynamic parameters for the binding between MB and G_9 were calculated from the van't Hoff equation.

2.6 Structural modeling.

The geometries of the molecular fragments of single strand DNA were obtained at the density functional theory (DFT) level using the B3LYP functional and 6-31G(d,p) basis set [45,46] using Gaussian 03 [47] package. To limit the size of each fragment whilst maintaining representativeness, fragments were modeled with three nucleotides with a phosphate group added to the 5' end. A methyl group was also added to the phosphate groups of 5' and 3' in order to maintain the phosphodiester structure.

3 Results and Discussion

3.1 UV-VIS absorption experiments

Figure 1a shows the absorption spectra of MB in the 500-800 nm region alone and in the presence of G_9. MB exists in the form of monomer and H-type dimer in aqueous

solution corresponding to two absorption bands with maxima at 665 and 600 nm respectively [14]. These bands are clearly visible in Figure 1a, indicating the predominant existence of the monomeric form under our experimental conditions (10 mM MB in Tris buffer pH 7.4 + 10 mM NaCl).

According to the literature [3], a hypochromic effect have been observed in the interaction of intercalative dyes with double-stranded DNA accompanied by a displacement of the absorption peak to higher wavelengths. These effects have been suggested to be due to the interaction between the electronic states of the dye and the DNA bases. In our case, the hypochromic effect observed upon addition of G_9 is associated with a very small bathochromic shift of the absorption maximum ($\Delta\lambda_{max}$ = 2 nm), in contrast to what is observed with double stranded DNA, indicating an interaction different to intercalative binding [3]. In similar experiments where the A_9, C_9, and T_9 single stranded DNA sequences were used, significantly lower effects on the intensities of the bands were observed (Figure 1b), signifying that the interaction of MB with guanine is favored, agreeing with previous reports for other MB-DNA systems [21-23].

Figure 1.

3.2 Fluorescence experiments.

Figure 2 shows the variations in the fluorescence spectra of MB upon addition of increasing concentrations of G_9 to a MB solution at room temperature. The excitation wavelength was set at 665 nm (monomer absorption band). As can be seen, the emission of MB is significantly quenched (~60%) upon addition of the same concentration of G_9, indicating a strong interaction of MB with the quencher i.e. DNA.

Figure 2.

Information on the stoichiometry of the complex was obtained from fluorescence data using the modified Benesi-Hildebrend equation [48] :

$$1/F_0\text{-}F = 1/ F_0\text{-}F_1 + 1/(F_0\text{-}F_1) K_g[G_9] \quad \text{Eq. 1}$$

where F_0 is the intensity of free MB, F_1 the intensity of complex MB-G_9, F the intensity of the mixture and Kg is the ground state association constant for the 1:1 complex formation. The linear B-H plot obtained, (Figure 2 inset), indicates that complex has a 1:1 stoichiometry and the value of K_g (1.5×10^5 M^{-1}) reveals a strong MB-G_9 association.

In contrast, the quenching effects in the case of A_9, C_9 and T_9 are lower than 8%, demonstrating selective quenching of MB by guanine-rich DNA sequences and agreeing well with the results observed using UV-VIS spectroscopy.

The steady-state fluorescence data obtained was analyzed using the Stern-Volmer equation [49] :

$$F_0/F = 1+ K_{SV}[Q] \quad \text{Eq. 2}$$

where F_0 and F are the fluorescence intensities in the absence and in the presence of quencher, respectively, K_{SV} is the Stern-Volmer quenching constant and [Q] is the quencher concentration. The Stern-Volmer plots for the quenching of MB with the studied DNA sequences are shown in Figure 3a. The quenching profiles obtained follow a linear dependence on quencher concentration, indicating a fundamental contribution

of either collisional or static type quenching [48,49]. The higher K_{SV} value for the MB-G_9 system indicates a stronger interaction of MB. The Stern-Volmer quenching constant K_{SV} values decrease as the temperature increases (Figure 3b), indicating that static quenching has a fundamental influence on the overall quenching mechanism, due to the increase in temperature that reduces the stability of the complex, resulting in lower static quenching constants.

In this situation, the quenching data were analyzed according to the modified Stern-Volmer equation [49-51] :

$$F_0/\Delta F = 1/f_a K_a [Q] + 1/f_a \qquad \text{Eq.3}$$

where ΔF is the difference in fluorescence in the absence and in the presence of the quencher, f_a being the fraction of the total fluorophore accessible to the quencher and K_a is the quenching constant. The dependence of $F_0/\Delta F$ on the reciprocal value of the quencher concentration $[Q]^{-1}$ is linear with a slope of $1/f_aK_a$, with the f_a value is fixed on the ordinate. The modified Stern-Volmer plot obtained for the interaction of MB with G_9 at 298 K is shown in Figure 3c, from which $K_a = 3.6 \times 10^5\ M^{-1}$ and $f_a = 0.96$ were calculated. The K_a values for different temperatures are detailed in Table 1, a trend of decreasing K_{SV} with increasing temperature is observed, in agreement with the K_a temperature dependence. As expected the f_a is close to 1, as the fluorophore in solution is always accessible to the quencher in this temperature range.

The thermodynamic parameters for the binding between MB and G_9 were calculated from the van't Hoff equation (Eq. 4) [52] :

$$\ln K_a = - \Delta H/RT + \Delta S/R \qquad \text{Eq. 4}$$

where ΔH is the enthalpy change (which is considered constant in the temperature range studied), ΔS is the entropy change, K_a has a similar physical meaning as the effective quenching constant K_a at the corresponding temperature and R is the ideal gas constant.

Figure 3

The linear dependence obtained for the van't Hoff plot (Figure 4) using the data included in Table 1 shows that the assumption of near constant ΔH is correct.

Figure 4.

The enthalpy change (ΔH) is calculated from the slope of the van't Hoff relationship and the free energy change (ΔG) is then estimated from:

$$\Delta G = \Delta H - T\,\Delta S \qquad \text{Eq. 5}$$

The values of ΔH and ΔS obtained and the ΔG values calculated for each temperature are also shown in Table 1. The negative values of ΔG support the spontaneous character of the binding interaction. In agreement with the Roos and Subramanian model [53] enthalpy change and the positive entropy of the MB-G_9 interaction indicate that the electrostatic effect plays a major role in the binding process.

3.3 Ionic strength dependence

In order to further clarify the binding mode, the fluorescence responses of MB in the presence of G_9 was studied in 10 mM Tris·HCl pH 7.4 at different concentrations of LiCl, NaCl, KCl, $MgCl_2$ and NBu_4Cl.

Table 2 correlates the hydrated ionic radii (r_{hyd}) of the studied cations [54] with the variation of F/F_0 at 1:1 MB:G_9 molar ratio at increasing ionic strengths. As can be seen, the quenching effect of G_9 on the fluorescence of MB decreased as the concentrations of monopositive ion salts increased. This result supports the hypothesis of an electrostatic binding, as at high ionic strength the negative charge of G_9 is partially neutralized by the monopositive cations, thus blocking the electrostatic interaction with the positive centers of MB.

At low concentrations of Li^+ (hydrated ionic radius r_{hyd} = 382 pm) or Na^+ (r_{hyd} = 358 pm) there is a strong quenching effect, which can be interpreted as the result of the competition between the hydrated monocations with H_3O^+ (r_{hyd} = 280 pm) in their interactions with G_9, which favours H_3O^+ at this low salt concentration. Concomitantly, the large volume of the hydrated cation blocks the adjacent sites to those that each cation occupies in its binding to the DNA molecule.

The charge effect is more significant when the quenching process was studied in the presence of Mg^{2+} (r_{hyd} = 428 pm). In this case, although the hydrated ionic radius is bigger, this divalent cation provoked only a 10% quenching at Mg^{2+} concentrations as low as 10 mM. As expected, the MB-G_9 interaction is almost independent of NBu_4^+ concentration, due to the weak binding character of bulky tetraalkylammonium ions and confirming the markedly electrostatic character of the MB-G_9 interaction.

The obtained values of F/F_0 for K^+ can be interpreted in terms of the formation of a G-quadruplex structure, which is favoured even in the presence of low concentrations of

this ion. This effect is also expected to contribute to the quenching behaviour in the presence of high Na^+ concentrations [40-43].

3.4 Effect of pH on the fluorescence changes

The dependence of the fluorescence changes with pH also supports the electrostatic nature of the MB-G_9 interaction (Figure 5). In all cases the increment in G_9 concentration causes a decrease of F/F_0 ratio, with a less marked effect at acidic pH (in 10 mM citrate buffer pH 3). At pH 7.4, the DNA phosphate backbone is almost completely ionized (assuming a pK_a value for the phosphodiester group of 2, the degree of protonation is lower than 0.001%) [55], which allows the electrostatic interaction of the polyanionic sequence with MB^+ diminishing the fluorescence sensitivity. In contrast, at pH 3 the degree of protonation increases up to 10% and consequently the quenching effect is lower.

Figure 5.

3.5 DFT calculations on the interaction of MB with single stranded DNA

The experimental results were also interpreted in terms of a prevalence of the electrostatic interaction between the MB and the single-stranded DNA fragments. Theoretical methods such as the density functional theory offer the possibility to understand the structural features of molecular architectures. Figure 6 shows the optimized geometries corresponding to molecular fragments having three identical nucleotides (GGG, CCC, AAA and TTT) calculated, taking into consideration that at pH 7.4 the DNA phosphate backbone is fully ionized. The arrows indicate the region of more negative electronic density and it can be seen that the internal phosphate groups in

GGG are located in a more accessible position, with the steric effects facilitating the electrostatic interaction between the MB^+ with this fragment. This effect is less evident in the other three structures, which is in agreement with our experimental results.

Figure 6.

4. Conclusions

In the work reported here, fluorescence techniques have been exploited to demonstrate that the interaction of MB with single stranded DNA occurs essentially with the 2'-deoxyguanine 5'-phosphate nucleotide, as evidenced by the higher quenching effect of G_9. According to the Stern-Volmer plots, static quenching is the principal mechanism for the observed MB fluorescence quenching mechanism in the presence of single-stranded DNA. Furthermore, the thermodynamic parameters obtained with the van't Hoff equation and the effect of ionic strength indicates a highly electrostatic contribution to the binding process. In the case of the interaction of MB with DNA in the presence of K^+, the formation of secondary structures (G-quadruplex) cannot be ruled out. Finally, quantum chemical modeling at DFT//B3LYP/6-31G(d,p) level confirms the experimental results. These results not only provide a clear insight into the interaction between methylene blue and DNA but can also be exploited for the design of novel DNA sensors based on photoactive labels.

Acknowledgements

This work has been carried out with financial support from the Commission of the European Communities specific RTD programme FP7-2008-ICT-216031 CD-MEDICS. AF thanks Ministerio de Ciencia e Innovación, Spain, for a "Ramón y Cajal" Research

Professorship. PJO thanks the Departament d'Enginyeria Química, Universitat Rovira i Virgili, for a Visiting Professorship.

References

[1] C. F. Yang, P. J. Jackson, Z. Xi, I. H. Goldberg, Recognition of Bulged DNA by a Neocarzinostatin Product via an Induced Fit Mechanism, Bioorg. Med. Chem. 10 (2002) 1329-1335.

[2] H. Junicke, J. R. Hart, J. Kisko, O. Glebov, J. R. Barton. A rhodium(III) complex for high-affinity DNA base-pair mismatch recognition, Proc. Natl. Acad. Sci. 100 (2003) 3737-3742.

[3] L. Z. Zhang, G. Q. Tang. J. Photochem. Photobiol, The binding properties of photosensitizer methylene blue to herring sperm DNA: a spectroscopic study, B 74 (2004) 119-125.

[4] J. Rengelshausen, J. Burhenne, M. Fröhlich, Y. Tayrouz, S. K. Singh, K. Riedel, O. Müller, T. Hoppe-Tichy, W. E. Haefeli, G. Mikus, I. Walter-Sack, Evaluation of pharmacokinetic interaction between cetirizine and ritonavir, an HIV-1 protease inhibitor, in healthy male volunteers, Eur. J. Clin. Pharmacol, 74 (2004) 709-715.

[5] E. C. Long, J. K. Barton, On demonstrating DNA intercalation, Acc. Chem. Res. 23 (1990) 271-273.

[6] B. S. Fujimoto, J. B. Clendenning, J. J. Delrow, P. J. Heath, M. Schurr, Fluorescence and Photobleaching Studies of Methylene Blue Binding to DN, J. Phys. Chem. 98 (1994) 6633-6643.

[7] E. Tuti, B. Norden, Sequence-Specific Interactions of Methylene Blue with Polynucleotides and DNA: A Spectroscopic Study, J. Am. Chem. Soc. 116 (1994) 7548-7556.

[8] B. Armitage, Photocleavage of Nucleic Acids, Chem Rev. 98 (1998) 1171-1200.

[9] D. Li, Y. Yan, A. Wieckowska, I. Willner, Amplified electrochemical detection of DNA through the aggregation of Au nanoparticles on electrodes and the incorporation of methylene blue into the DNA-crosslinked structure, Chem. Comm. (2007) 3544-3546.

[10] S. F. Baranovskii, P. A. Bolotin, M. P. Evstigneev, D. N. Chernyshev, Complexation of heterocyclic ligands with DNA in aqueous solution, J. Appl. Spect. 75 (2008) 251-260.

[11] T. J. Bride, J. E. Schneider, R. A. Floyd, L. A. Loeb, Mutations induced by methylene blue plus light in single-stranded M13mp2, Proc. Natl. Acad. Sci. 89 (1992) 6866-6870.

[12] M. Pádula, S. Boiteux, Mutations induced by methylene blue plus light in single-stranded M13mp2, J. Med. Biol. Res. 32 (1999) 1063-1071.

[13] D. Severino, H. C. Junqueira, M. Gugliotti, D. S. Gabrielli, M. S. Baptista. Influence of Negatively Charged Interfaces on the Ground and Excited State Properties of Methylene Blue, Photochem. Photobiol. 77 (2003) 459-468.

[14] D. Gabrielli, E. Belisle, D. Severino, A. J. Kowaltowski, M. S. Baptista, Binding, aggregation and photochemical properties of methylene blue in mitochondrial suspensions, Photochem. Photobiol.79 (2004) 227-232.

[15] Y .Ni, D. Lin, S. Kokot, Synchronous fluorescence and UV–vis spectroscopic studies of interactions between the tetracycline antibiotic, aluminium ions and DNA with the aid of the Methylene Blue dye probe, Anal. Chim. Acta. 606 (2008) 19-25.

[16] R. Rohs, H. Sklenar, Blue Binding to DNAwith Alternating AT Base Sequence: Minor Groove Binding is Favored over Intercalation, J. Biomol. Struct. Dyn. 21 (2004) 699-711.

[17] R. Rohs, H. Sklenar, R. Lavery, B. Röder, Methylene Blue Binding to DNA with Alternating GC Base Sequence: A Modeling Study, J. Am. Chem. Soc. 122 (2000) 2860-2866.

[18] R. M. Anson, D. L. Croteau, R. H Strerum, C. Filburn, R. Parsell, V. A. Bohr, Homogenous repair of singlet oxygen-induced DNA damage in differentially transcribed regions and strands of human mitochondrial DNA, Nucleic Acids Res. 26 (1998) 662-668.

[19] H. Ch. DeFedericis, H. B. Patrzyc, M. J. Rajecki, E. E. Budzinski, H. Iijima, J. B. Dawidzik, M. S. Evans, Singlet Oxygen-Induced DNA Damage, Radiat. Res.165 (2006) 445-451.

[20] S. N. Kassam, A, J. Rainbow, Deficient base excision repair of oxidative DNA damage induced, Biochem. Biophys. Res. Commun.359 (2007) 1004-1009.

[21] D. C. Malins, N. L. Polissar, G. K. Ostrander, M. A. Vinson, Single 8-oxo-guanine and 8-oxo-adenine lesions induced marked changes in yhe backbone structure of a 25-base DNA strand, Proc. Natl. Acad. Sci. 97 (2000) 12442-12445.

[22] Y. Zheng, J. R. Wagner, L. Sanche. Singlet Oxygen-Induced DNA Damage, Phys. Rev. Lett. 96 (2006) 208101-208104.

[23] S. Nishimura. 8-Hydroxyguanine: From its discovery in 1983 to the present status, Proc. Jpn. Acad. Ser .B 82 (2006) 127-141.

[24] W. Yang, M. Ozsoz, D. B. Hibbert, J. J. Gooding, Evidence for the Direct Interaction Between Methylene Blue and Guanine Bases using DNA-Modified Carbon Paste Electrodes, Electroanalysis 14 (2002) 1299-1302.

[25] E. Farjami, L. Clima, K. V. Gothelf, E. E. Ferapontova, DNA interactions with a Methylene Blue redox indictor depend on the DNA length and are sequence specific, Analyst 135 (2010) 1443-1448.

[26] D. Pau, X, Zuo, Y. Wan, L. Wang, J. Zhang, S. Song, C. Fan, Electrochemical Interrogation of Interctions between Surface-Confined DNA and Methylene Blue, Sensors 7 (2007) 2671-2680.

[27] O. Y. F. Henry, J. L. Acero Sánchez, D. Latta, C. K. O'Sullivan, Electrochemical quantification of DNA amplicons via the detection of non-hybridised guanine bases on low-density electrode arrays, Biosens. Bioelectron. 24 (2009) 2064–2070.

[28] Z. Hu, C. L. Tong, Synchronous fluorescence determination of DNA based on the interaction between methylene blue and DNA, Anal. Chim. Acta, 587 (2007)187–193.

[29] H. Ihmels, D. Otto. Intercalation of Organic Dye Molecules into Double-Stranded DNA : General Principles and Recent Developments, Top. Curr. Chem. 258 (2005) 161–204.

[30] J. Shen, T. Yu, J. Xie, Y. Jiang. Photoluminescence of CdTe nanocrystals modulated by methylene blue and DNA. A label-free luminescent signaling nanohybrid platform, Phys. Chem. Chem. Phys.11 (2009) 5062-5069.

[31] H. Reza, S. Nafiseh, P. Afsaneh. DNA-binding Studies of Daunorubicin in the Presence of Methylene Blue by Spectroscopy and Voltammetry Techniques, Chin. J. Chem.27 (2009) 1055-1060.

[32] Y. Ni, D. Lin, S. Kokot, Synchronous fluorescence and UV–vis spectroscopic studies of interactions between the tetracycline antibiotic, aluminium ions and DNA with the aid of the Methylene Blue dye probe, Anal. Chim. Acta 606 (2008) 19-25.

[33] Y. Wang, A. Zhou, Spectroscopic studies on the binding of methylene blue with DNA by means of cyclodextrin supramolecular systems, J. Photochem. Photobiol. A: Chem.190 (2007)121-127.

[34] S. Hongxia, X. Junfeng, Z. Yazhou, X. Guangshi, X. Lianghua , T. Talin, Spectroscopic studies of the interaction between methylene blue and G-quadruplex, Chin. Sci. Bull.51 (2006) 1687-1692

[35] G. N. Parkinson, P. H. Lee, S. Neidle, Crystal structure of parallel quqdruplexes from human telomeric DNA, Nature 417 (2002) 876-880.

[36] W. C. Wong, J. Zhang, S. L. Ling, L. L. Lin, S. Hiew, J. Guo, Z. Yang, T. Li, Conformational organization of G-quadruplexes composed of $d(G_4T_n)_3G_4$, Bioorg. Med. Chem. Lett. 20 (2010) 4689- 4692.

[37] F. Rose, V. Gabelica, H. Poncelet, E. DePauw, Tetramolecular G-quadruplexes formation pathways studied by electrospray mass spectrometry, Nucl. Acids Res.38 (2010) 5217-5225.

[38] P. Sket, J. Plavee., Tetramolecular DNA Quadruplexes in Solution: Insights into Structural Diversity and Cation Movement, J. Am. Chem. Soc. 132 (2010) 12724-12732.

[39] M. H. Li, Q. Luo, X. G. Xue, Z. S. Li, Toward a full structural characterization of G-quadruplex DNA in aqueus solution : Molecular dynamic simulation of four G-quadruplex molecules, J. Mol. Struc.: Theochem. 952 (2010) 96-102.

[40] A. T. Phan, D. J. Patel, Two-repeat Human Tolomeric d(TAGGGTTGGGT) Sequences Forms Interconverting Parallel and Antiparallel G-Quadruplexes in Solutions: Distinct Topologies, Thermodinamics Properties and Folding/Unfolding Kinetics, J. Am. Chem, Soc. 125 (2003) 15021-15027.

[41] S. Burge, G. N. Parkinson, P. Hazel. A. K. Todel. S. Neidle, Quadruplex DNA : sequence, topology and structure, Nucl. Acids Res. 34 (2006) 5402-5411.

[42] J. L. Huppert, Four-stranded nucleic acid: structure, function and targeting of G-quadruplexes, Chem. Soc. Rev.37 (2008) 1375-1393.

[43] Y. Quin, L. H. Hurley, Structures folding patters, and function of intramolecular DNA G-quadruplexes found in enkaryotic promoter regions, Biochimie 90 (2008) 1149-1171.

[44] K. Bergmann, C. T. O'Conski, A spectroscopic study of methylene blue monomer, dimer and complexes with montmorillonite, J. Phys. Chem. 67 (1963) 2169-2177.

[45] W. Kohn, L. Sham. L. Sham, Self-Consistent Equations Including Exchange and Correlation Effects, Phys. Rev. 140 (1965) A1133-A1138.

[46] P. J. Stephan, F. J. Devlin, C. F. Chavalowski, M. J. Frisch, Theoretical and experimental study of the conformational, structural analysis and vibrational spectra of 1,2-bis(1,2,4-triazole-1-yl)ethane, J. Phys. Chem. 98 (1994)11623-11630.

[47] M. J. Frisch, G.W. Trucks, H. B. Schlegel, G. E. Scuseria, M. A. Robb, J. R. Cheeseman, J. A. Montgomery, Jr. T. Vreven, K. N. Kudin, J. C. Burant, J. M. Millam, S. S. Iyengar, J. Tomasi, V. Barone, B. Mennucci, M. Cossi, G. Scalmani, N. Rega, G. A. Petersson, H. Nakatsuji, M. Hada, M. Ehara, K. Toyota, R. Fukuda, J. Hasegawa, M. Ishida, T. Nakajima, Y. Honda, O. Kitao, H. Nakai, M. Klene, X. Li, J. E. Knox, H. P. Hratchian, J. B. Cross, C. Adamo, J. Jaramillo, R. Gomperts, R. E. Stratmann, O. Yazyev, A. J. Austin, R. Cammi, C. Pomelli, J. W. Ochterski, P. Y. Ayala, K. Morokuma, G. A. Voth, P. Salvador, J. J. Dannenberg, V. G. Zakrzewski, S. Dapprich, A. D. Daniels, M. C. Strain, O. Farkas, D. K. Malick, A. D. Rabuck, K. Raghavachari, J. B. Foresman, J. V. Ortiz, Q. Cui, A. G. Baboul, S. Clifford, J. Cioslowski, B. B. Stefanov, G. Liu, A. Liashenko, P. Piskorz, I. Komaromi, R. L. Martin, D. J. Fox, T. Keith, M. A. Al-Laham, C. Y. Peng, A. Nanayakkara, M. Challacombe, P. M. W. Gill, B. Johnson, W. Chen, M. W. Wong, C. Gonzalez, J. A. Pople, Gaussian 03, Revision C.02, Gaussian, Inc., Pittsburgh PA, 2003.

[48] S. Mitra, R. Das, S. J. Mukherjee, Proton Transfer in Inclusion Complexes of Cyclodextrins: Role of Water and Highly Polar Nonaqueous Media, J. Phys. Chem. B 102 (1998) 3730-3737.

[49] B. Valeur, Molecular Fluorescence: Principles and Applications, Wiley-VCH, Heidelberg, Chapter 4, 2001.

[50] H. R. Park, J. J. Seo, S. C. Chin, H. S. Lee, K. M. Bark, Fluorescence Quenching of Norfloxacin by Divalent Transition Metal Cations, Bull. Kor. Chem. Soc. 28 (2007) 1573-1578.

[51] K. S. Shashidhara, S. M. Gaikwad, Fluorescence Quenching and Time-resolved Fluorescence studies of α-Mannosidase from Aspergillus fischeri (NCIM 508), J. Fluoresc.17 (2007) 599-605.

[52] P Atkins, J. de Paula, Physical Chemistry, 8th Edition, Oxford University Press, New York. Chapter 9, 2006.

[53] P. Ross, S. Subramanian, Thermodynamics of protein association reactions: forces contributing to stability, Biochemistry 20 (1981) 3096-3102.

[54] A. G. Volkov, S. Paula, D. W. Deamer, Two mechanisms of permeation of small neutral molecules and hydrated ions across phospholipid bilayers, Bioelectrochem. Bionerg. 42 (1997) 153-160.

[55] A. C. Hengge, W. W. Cleland, Phosphoryl-transfer reactions of phosphodiesters: characterization of transition states by heavy-atom isotope effects, J. Am. Chem. Soc. 113 (1991) 5835-5841.

Figure captions

Scheme 1. Molecular structure of methylene blue.

Figure 1. (a) Absorption spectra of MB and MB-G_9 at 298 K (c(DNA) = 10 μM, buffer: 10 mM Tris-HCl pH 7.4. + 10 mM NaCl) (b) Dependence of A/A_0 (at 665 nm) with the studied oligonucleotides (A_9, C_9, G_9 and T_9) at different molar ratios.

Figure 2. Fluorescence spectra of MB recorded in the absence and in the presence of increasing concentrations of G_9 at 298 K (λ_{exc}= 665 nm). Inset: Modified Benesi-Hildebrand plot.

Figure 3. a) Stern-Volmer plot of the MB fluorescence in the presence of the studied sequences at 298 K: G_9 (▲), A_9 (●), C_9 (■), T_9 (▼). b) Stern-Volmer behavior of MB-G_9 system at different temperatures. c) Modified Stern-Volmer plot of MB-G_9 system at 298 K.

Figure 4. van´t Hoff plot for MB-G_9 system.

Figure 5. Effect of pH on F/F_0 (at 686 nm) for MB-G_9 system at different molar ratios.

Figure 6. Structural models obtained at DFT level using the B3LYP functional and 6-31G (d,p) basis set for the single stranded DNA fragments.

Table 1. The effective quenching constant (K_a), the fraction of accessible fluorophore (f_a) and thermodynamic parameters of MB-G_9 system calculated at different temperatures.

T/K	**$K_a/10^5$ M^{-1}**	**f_a**	**ΔH/kJ.mol^{-1}**	**ΔS/J.mol^{-1}.K^{-1}**	**ΔG/kJ.mol^{-1}**
288	4.0	0.98	-5.70	87.2	-30.8
293	3.8	0.96			-31.3
298	3.6	0.93			-31.7
303	3.5	0.92			-32.1
308	3.4	0.88			-32.6
313	3.3	0.87			-32.9

Table 2. Variation of F/F_0 (at 686 nm) at 1:1 MB:G_9 molar ratio with increasing ionic strengths.

Ion	**r_{hyd} (pm)[a]**	**F/F_0 (%)**		
		10 mM	**100 mM**	**1 M**
H_3O^+	280	-	-	-
K^+	331	60	75	86
Na^+	358	42	66	85
Li^+	382	44	75	90
Mg^{2+}	428	85	87	95
$[N(Bu)]_4^+$	-	40	45	47

[a] from reference [54].

Scheme 1

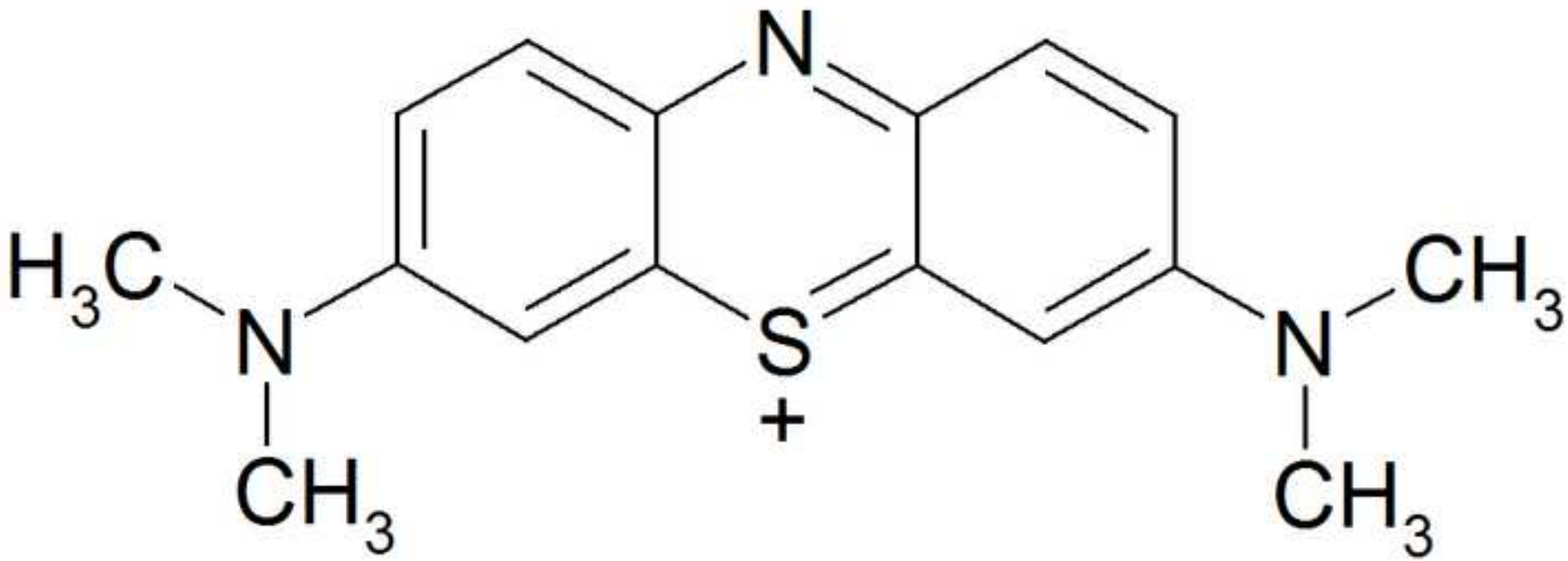

Figure 1

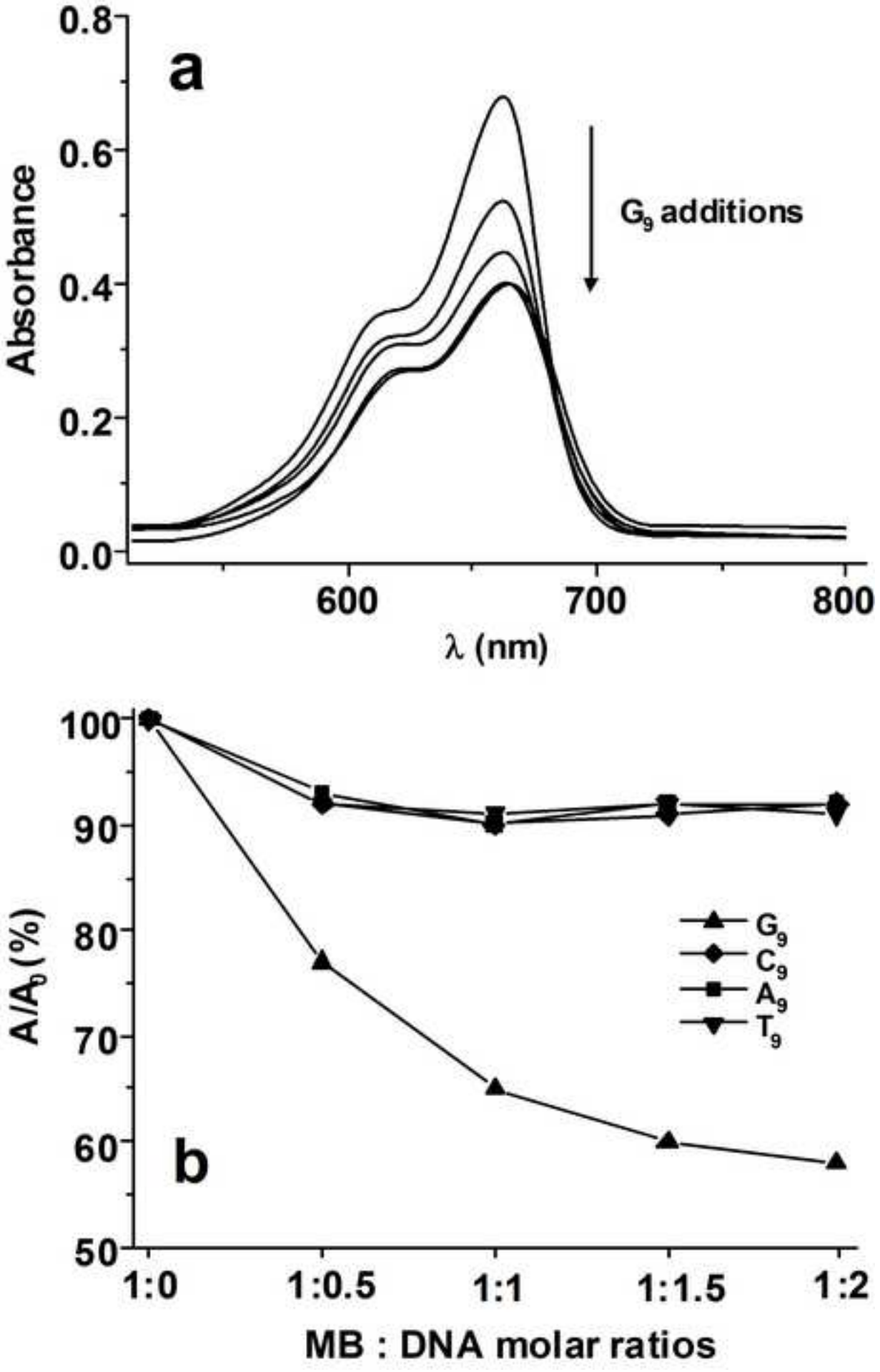
a
Absorbance
0.8
0.6
0.4
0.2
0.0
600
700
800
λ (nm)
G9 additions
b
A/A0 (%)
100
90
80
70
60
50
1:0
1:0.5
1:1
1:1.5
1:2
MB : DNA molar ratios
G9
C9
A9
T9

Figure 2

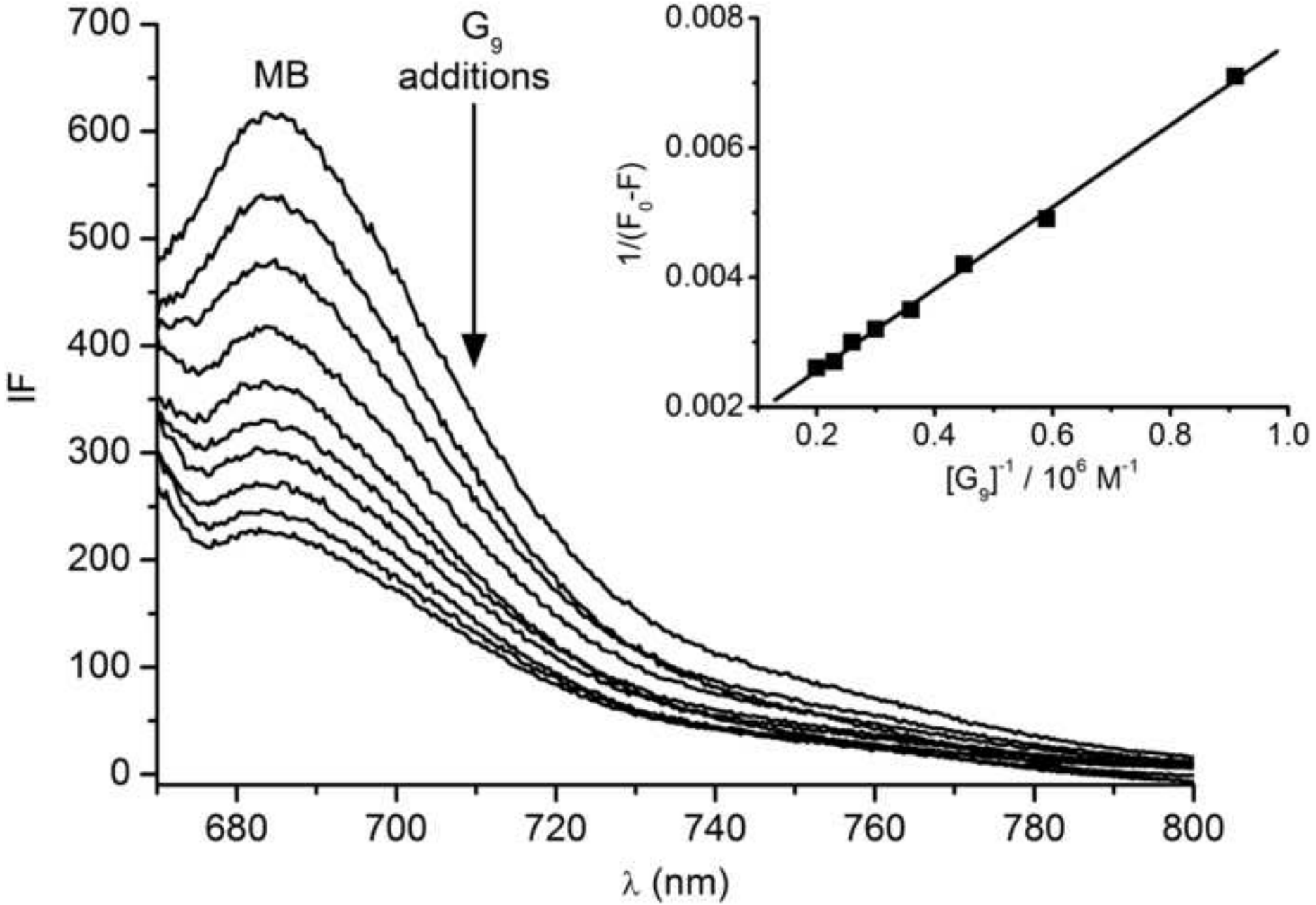

Figure 3

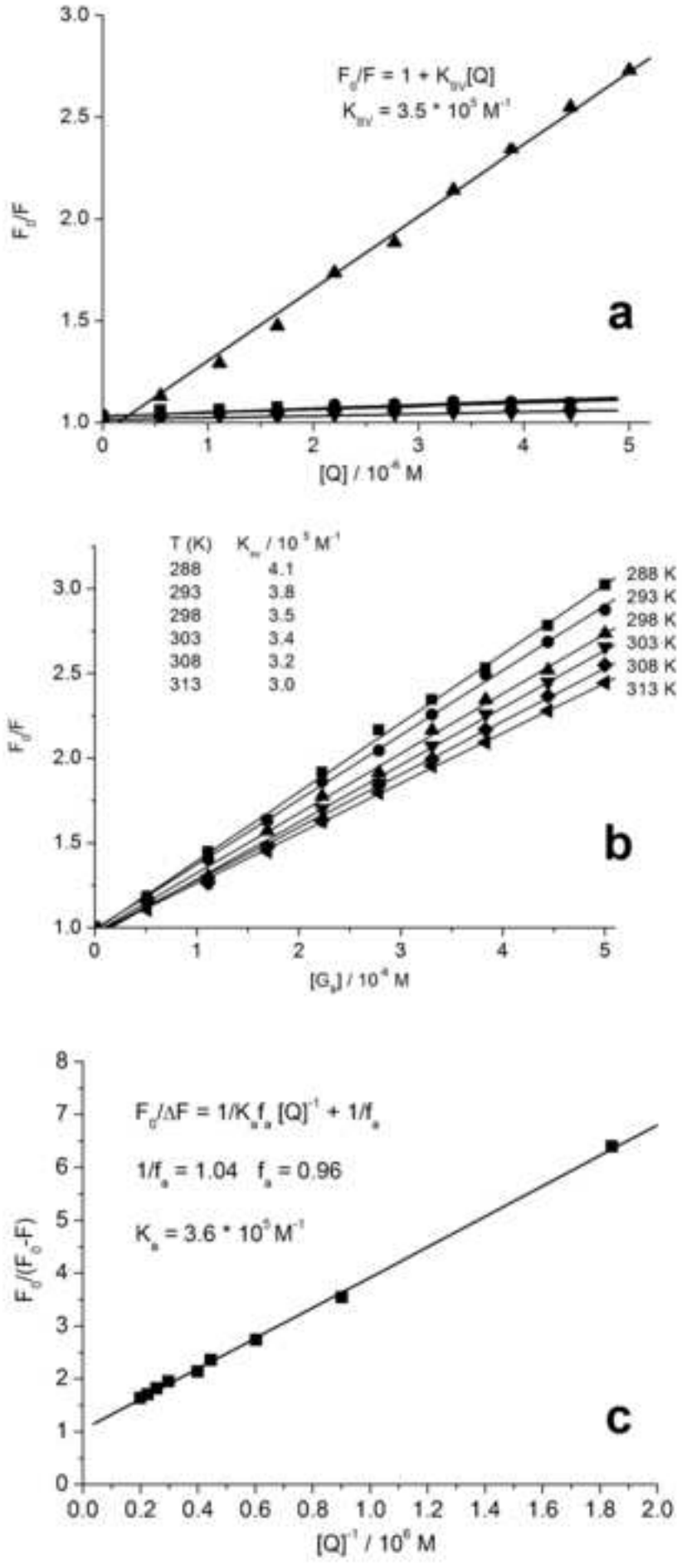
$F_0/F = 1 + K_{SV}[Q]$
$K_{SV} = 3.5 * 10^5\ M^{-1}$
a
F_0/F
[Q] / 10^{-6} M
T (K) K_{sv} / $10^5\ M^{-1}$
288 4.1
293 3.8
298 3.5
303 3.4
308 3.2
313 3.0
288 K
293 K
298 K
303 K
308 K
313 K
b
F_0/F
$[G_s]$ / 10^{-6} M
$F_0/\Delta F = 1/K_a f_a [Q]^{-1} + 1/f_a$
$1/f_a = 1.04$ $f_a = 0.96$
$K_a = 3.6 * 10^5\ M^{-1}$
c
$F_0/(F_0-F)$
$[Q]^{-1}$ / 10^6 M

Figure 4

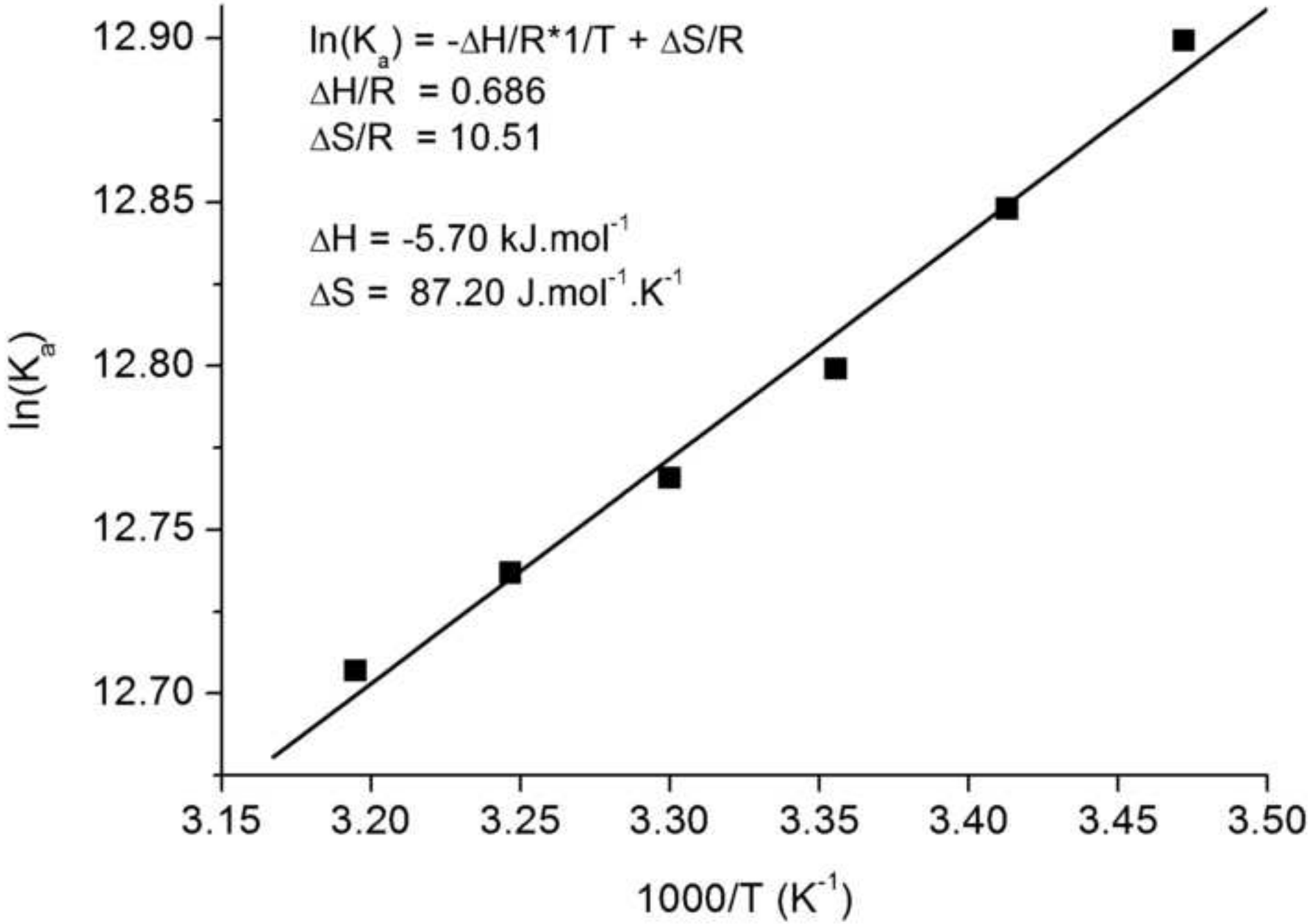
ln(K_a) = -ΔH/R*1/T + ΔS/R
ΔH/R = 0.686
ΔS/R = 10.51
ΔH = -5.70 kJ.mol^-1
ΔS = 87.20 J.mol^-1.K^-1
ln(K_a)
12.90
12.85
12.80
12.75
12.70
3.15
3.20
3.25
3.30
3.35
3.40
3.45
3.50
1000/T (K^-1)

Figure 5

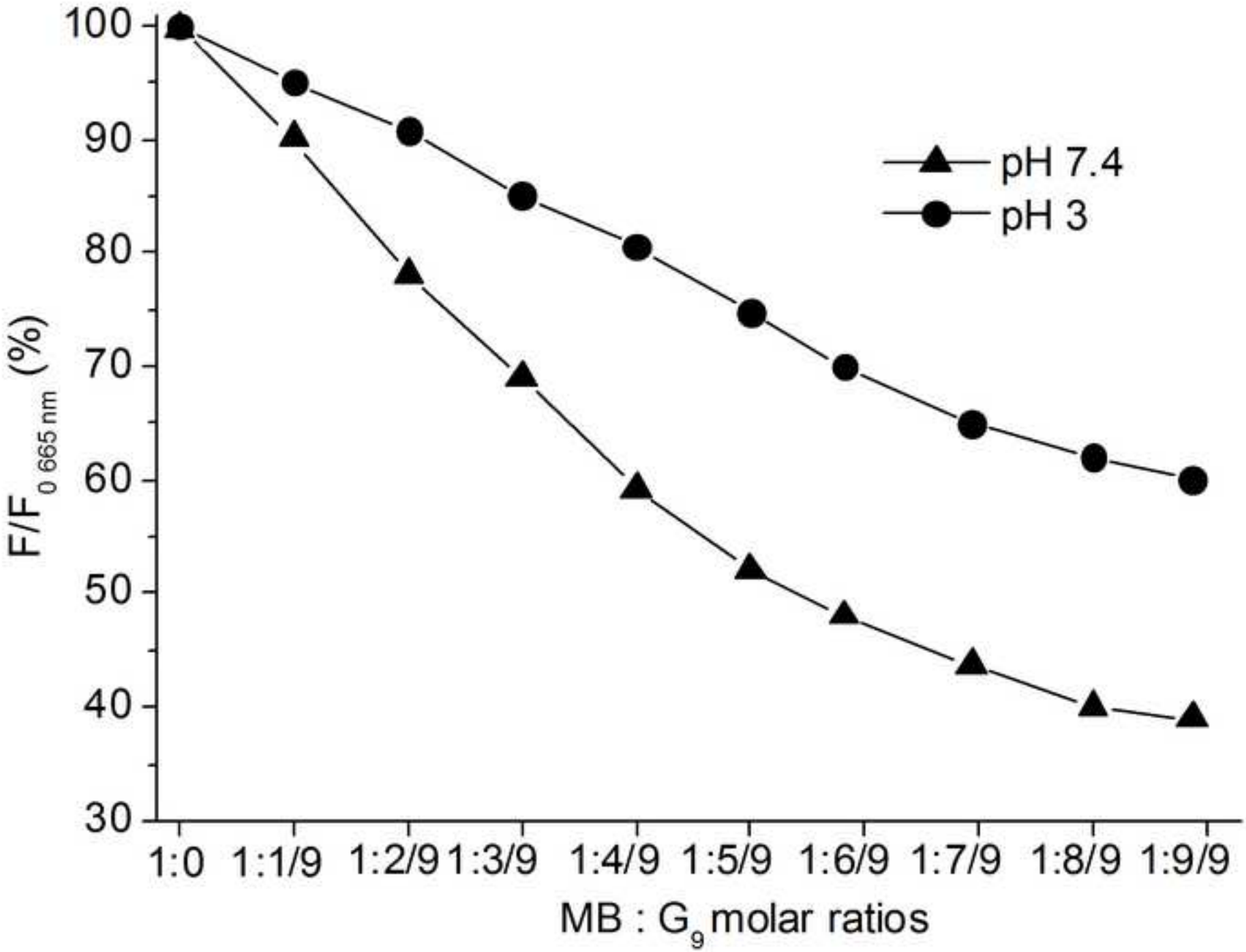
100
90
80
70
60
50
40
30
F/F0 665 nm (%)
pH 7.4
pH 3
1:0
1:1/9
1:2/9
1:3/9
1:4/9
1:5/9
1:6/9
1:7/9
1:8/9
1:9/9
MB : G9 molar ratios

Figure 6